Experimental and Numerical Study of High-Altitude Ignition of a Turbojet Combustor

NICOLÁS GARCÍA ROSA,[1] GUILLAUME LINASSIER,[2] RENAUD LECOURT,[2] PHILIPPE VILLEDIEU,[2] and GÉRARD LAVERGNE[2]

[1]ISAE, Université de Toulouse, Toulouse, France
[2]ONERA/DMAE, Université de Toulouse, Toulouse, France

This paper aims at contributing to the methodology used for the numerical prediction of ignition inside a combustion chamber. For this purpose, experiments are carried out in a model combustor with improved optical access. Laser tomography and high-speed video give a first insight into the unsteady airflow and the flame structure. Laser Doppler anemometry is used to measure the gas flow velocity field, and the nonreactive two-phase flow is studied in detail using particle Doppler analysis. The velocity field of the burning spray is measured using particle image velocimetry. Ignition tests are performed to evaluate the minimum global equivalence ratio. This in-depth database is used to validate RANS simulations conducted in parallel using the ONERA computational fluid dynamics (CFD) code CEDRE. The numerical model for transient, spherical kernel ignition, proposed in previous work, has been improved and fully implemented in CEDRE. A first parametric study has been conducted on a basic configuration consisting of three validation cases: a gaseous mixture, a monodisperse spray, and a polydisperse spray. These validation cases are inspired from previous studies found in the literature and give a better understanding of the basic phenomena involved in the first stages of flame propagation. This model is then used in combination with CEDRE to estimate the ignition probability of given spark-plug positions in a more realistic configuration: the MERCATO combustor.

INTRODUCTION

Spray ignition represents a phenomenon of great fundamental and practical interest and is an important feature in the design of turbojet combustors. For instance, in-flight re-light at high altitude is a safety requirement for jet engines, and cold engine startup at high-altitude helipads is determining for the versatility of helicopters. One of the most critical situations is startup at altitudes higher than 6000 m above mean sea level, where ambient pressure is as low as 0.5 bar, and air, fuel, and even engine parts are as cold as 233 K. Extending the operational range of air-breathing turbojets calls for the development of reliable numerical simulation tools to predict engine re-light range at the design stage, in order to reduce the overall design cycle of new prototypes.

Assuming the primary combustion zones to be a well-stirred (gaseous) reactor, lean and rich extinction limits can be determined, as shown in Figure 1 (adapted from [1]). For high-altitude conditions, the loading factor increases and stability and ignition ranges become narrow. On the other hand, those ranges strongly depend on two-phase flow phenomena and, as a consequence, on the spray quality and the injection performance.

For gas turbines, the most reliable and convenient mode of ignition is an electrical spark discharge that fairly efficiently converts electrical energy into heat concentrated in a relatively small volume. The ignition process can be divided into two main phases, ignition kernel formation and kernel propagation. Kernel formation (Figure 2) can be divided into two steps: energy deposition (spark discharge) and spherical flame expansion (small-scale flame propagation). Kernel propagation also takes place in two different length scales: kernel transport into a recirculation zone and, finally, flame propagation to the whole chamber.

The authors acknowledge the financial support and contributions from Turbomeca.

Address correspondence to Professor Gérard Lavergne, ONERA Centre de Toulouse, Université de Toulouse, 2 av. Edouard Belin, BP 4025, 31055 Toulouse Cedex 4, France. E-mail: gerard.lavergne@onera.fr

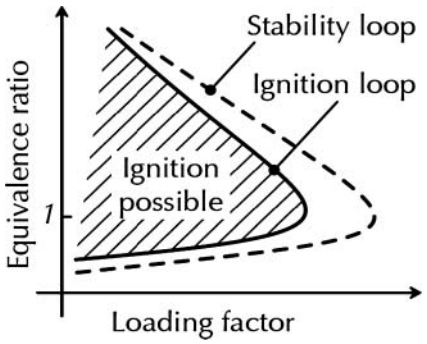

Figure 1 Example of combustor stability and ignition limits (adapted from Lefebvre [1]).

The wide range of time and length scales and the large number of physical phenomena involved in spray ignition are challenges that can be tackled by a combined analysis of experiments, numerical modeling, and numerical simulation.

EXPERIMENTAL STUDY

Experiments are carried out in a 130 × 130 × 250 mm rectangular model combustion chamber (Figure 3) with improved optical access (130 × 129 mm). The injection system, designed by Turbomeca, is composed of a pressure atomizer and an air swirler. The igniter can be placed on one of the windows, in eight different positions, relative to the injector plane (10, 23, 40, 53, 70, 83, 100, and 113 mm).

The combustor is mounted in the MERCATO test rig, which can simulate a wide range of ambient conditions. Air temperature can range from 240 K to 472 K, for a mass flow of 26 g/s, and liquid kerosene can be cooled down to 250 K. Air pressure can range from 0.4 bar to 4 bar.

The nonreactive airflow velocity field is characterized by two-component laser Doppler anemometry (LDA) measurements and the nonreactive spray is studied in detail using two-component particle Doppler analysis (PDA). Laser tomography

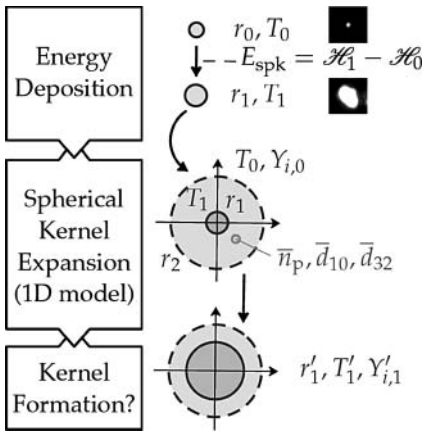

Figure 2 Ignition kernel formation.

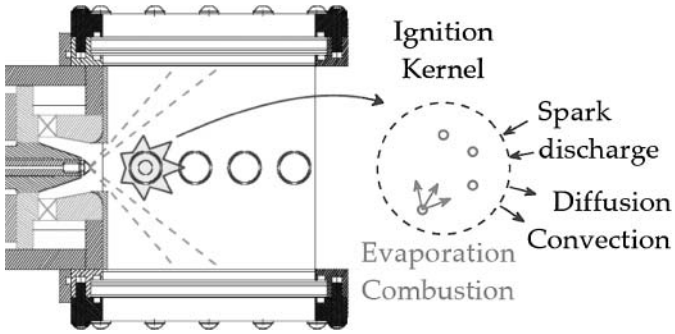

Figure 3 Experimental setup and definition of the ignition kernel.

and high-speed video give a first insight into the unsteady airflow and the flame structure, and the velocity field of the burning spray is measured using particle image velocimetry (PIV). This database is used to validate RANS simulations conducted in parallel using the ONERA computational fluid dynamics (CFD) code CEDRE.

The two-phase flow is ignited by a 400-mJ aviation-type spark plug, firing at a constant rate of approximately 4 Hz, with a spark duration of around 64 μs (Figure 4). Figure 4 shows a high-speed visualization of the spark discharge without fuel, as well as an estimation of the initial kernel size.

Figure 5 presents a 1-kHz visualization of the combustor ignition, showing the different phases of the ignition process: energy deposition and spherical expansion (between 0 and 1 ms), kernel transport (between 1 and around 12 ms), and subsequent flame spread (12 to 117 ms). Finally, Figure 6 shows the instantaneous spray structure before ignition, during kernel transport, and after flame stabilization. From Figure 6, one can easily understand the influence of the nonhomogeneous spray spatial distribution on the optimum position for the igniter. The burning spray is, naturally, more compact and concentrated in the vicinity of the injector, and thus the impacts on the windows are significantly reduced.

The lean ignition limit of the combustor (Figure 7) is determined by a series of ignition tests, conducted under atmospheric conditions, for different spark-plug positions. Among the different possible positions, the one at 70 mm has the lowest minimum injected equivalence ratio. This position is in the vicinity of the impact zone of the spray against the wall. Indeed, with the corner recirculation zone being fed with only the smallest droplets,

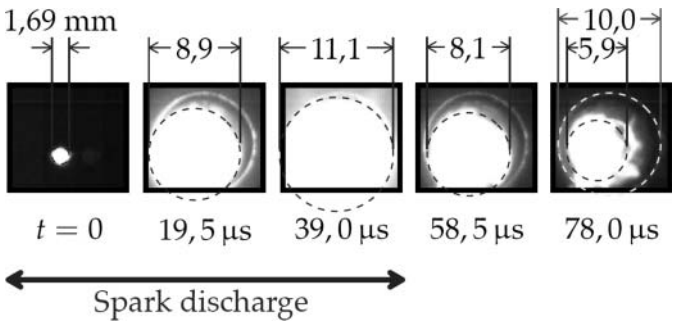

Figure 4 Ignition kernel formation by a spark discharge.

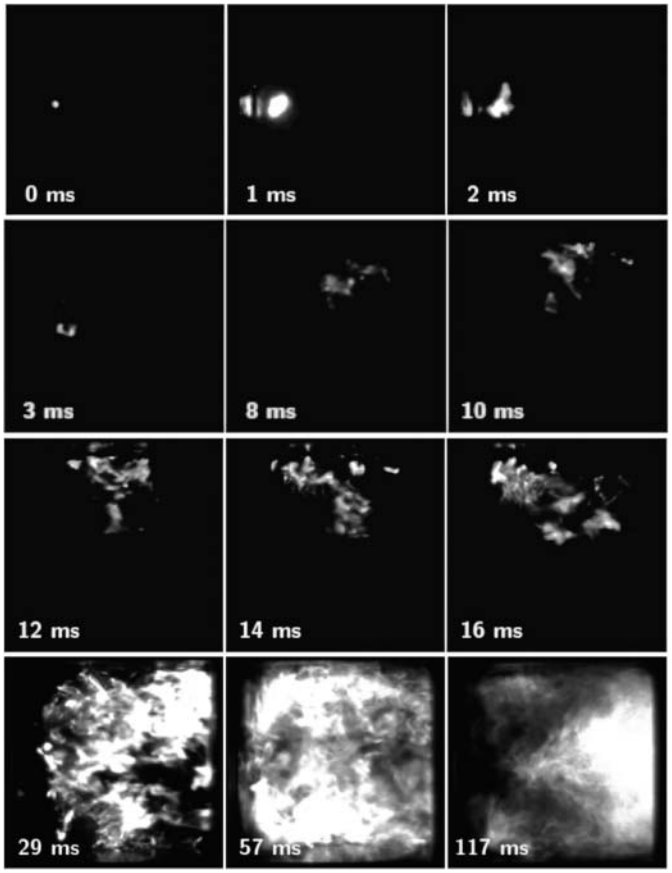

Figure 5 Visualization of combustor ignition (1 kHz).

the local equivalence ratio is lower, and a higher injected equivalence ratio is needed to ignite inside this region.

TWO-PHASE KERNEL IGNITION MODEL

With the objective of this work being the analysis of the influence of two-phase phenomena on ignition of air breathing engine combustors, the model presented here focuses on the initial stages of flame propagation. The detailed analysis of the spark discharge, as can be found in the literature [2], is therefore outside the scope of this paper.

Due to its very short duration (64 μs), the energy deposition phase is treated as an instantaneous, adiabatic heating process at constant pressure. Then heat diffusion, droplet evaporation, and

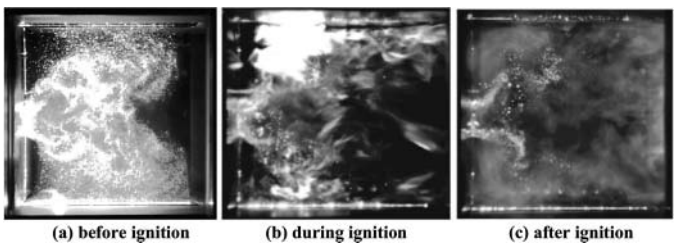

Figure 6 Laser tomography (10 Hz) of the spray before and after ignition.

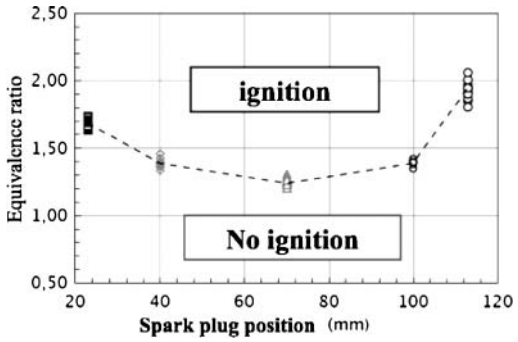

Figure 7 Lean ignition limit for the MERCATO combustor, (ambient conditions, air mass flow 26 g/s).

chemical reactions give birth to a spherical flame, which may grow or collapse, depending on the local equivalence ratio. The kernel growth phase is described by the numerical resolution of the conservation equations for a one-dimensional (1D) dilute spray mixture, inside the computational domain depicted by Figure 8, starting from the initial conditions given by the spark discharge phase.

Modeling Spark Discharge (Initial Conditions)

Let r_0 be the radius of the spherical volume containing the mass m_0 of mixture, at temperature T_∞, in which the spark energy E_{spk} is deposited. After deposition this volume will have expanded to radius $r_1 > r_0$ and temperature will have reached $T_1 > T_\infty$. Pressure is assumed to remain constant and the gaseous mixture is assumed to follow the ideal gas law, corrected by the compressibility factor Z [3], which accounts for dissociation effects at high temperature:

$$\frac{p}{\rho} = Z(T, p) \cdot r^0 \cdot T \tag{1}$$

The enthalpy balance

$$m_0 \left[h_g(T_1) - h_g(T_\infty)\right] = E_{spk} \tag{2}$$

can be rewritten using the ideal gas law to yield ($Z(T_\infty,p_\infty) = 1$)

$$\frac{4}{3}\pi r_0^3 \frac{p_\infty}{r^0 T_\infty}\left[h_g(T_1) - h_g(T_\infty)\right] = E_{spk} \tag{3}$$

Considering mass conservation $m_0 = m_1$, this expression yields

$$\frac{4}{3}\pi r_1^3 \frac{p_\infty}{Z(T_1, p_\infty) r^0 T_1}\left[h_g(T_1) - h_g(T_\infty)\right] = E_{spk} \tag{4}$$

Mass conservation and the enthalpy balance constitute a system of two equations, equivalent to the system of Eqs. (3) and (4), plotted in Figures 9a and b, for different values of E_{spk}. Unknowns are r_0, r_1, T_1, and E_{spk}. Indeed, although spark energy can be easily deduced from the voltage and current through the electrodes (400 mJ, in our case), a certain amount of energy

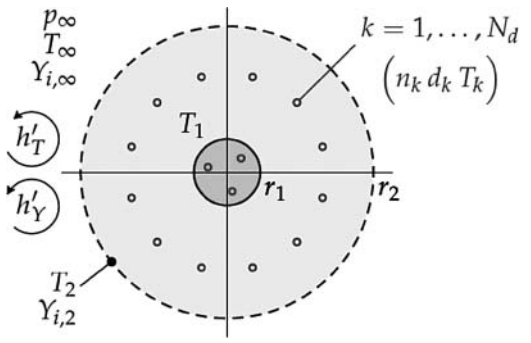

Figure 8 Computational domain for the numerical modeling of kernel growth.

is lost by heat conduction to the electrodes. Having only two equations and four unknowns, two of the unknowns must be determined through observation. Let us assume r_0 to be close to the spark gap ($r_0 \approx 2.2$ mm), and estimate $r_1 \approx 5.1$ mm from the high-speed visualizations presented in Figure 4. These two inputs are shown as vertical bands on Figures 9a and 9b. Using these plots, T_1 and E_{spk} are solved for, leading to a final temperature of 3500 K and a deposited energy of 200 mJ. The latter corresponds to a 50% heat loss to the electrodes, which is in agreement with observations from the literature.

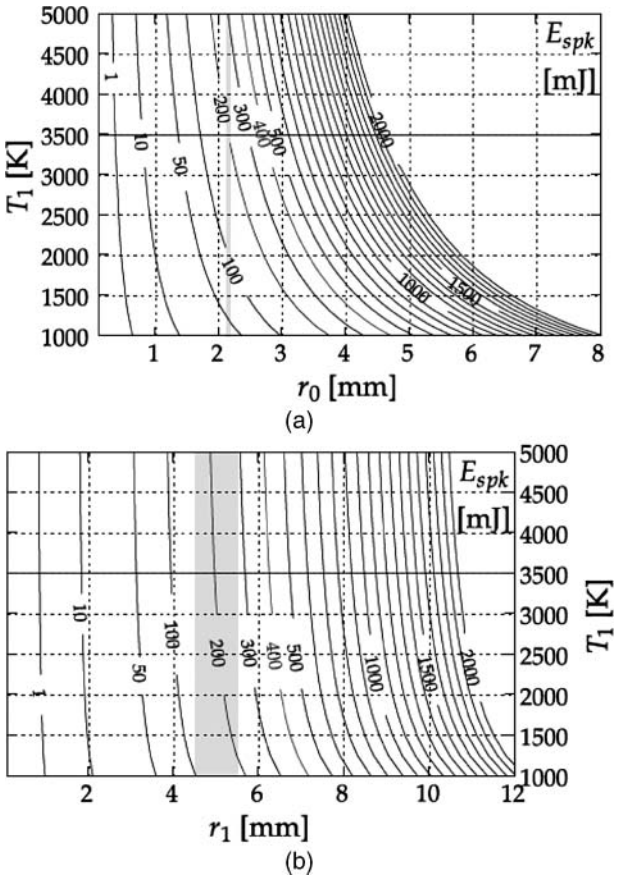

Figure 9 (a) Equation (3) for different values of E_{spk}. (b) Equation (4) for different values of E_{spk}.

Having determined T_1 and r_1, the initial conditions for the gas phase for kernel growth are

$$T_g(r,0) = \begin{cases} T_1 & amp; r \le r_1 \\ T_\infty & amp; r_1 < r \le r_2 \end{cases} \tag{5}$$

as shown in Figure 8. The composition of air at temperature T_∞ is taken for the initial composition and air and droplet velocities are zero.

Modeling Initial Kernel Growth

The gas phase of the mixture is represented by the 1D spherical mass and energy conservation equations, with multicomponent diffusion (Eqs. (6) to (8)), associated with the gas law of Eq. (1).

$$\frac{\partial \rho_g}{\partial t} + \frac{1}{r^2}\frac{\partial}{\partial r}\left(r^2 \rho_g u_r\right) = S_\rho \tag{6}$$

$$\rho_g \frac{\partial Y_i}{\partial t} + \rho_g u_r \frac{\partial Y_i}{\partial r} = \frac{1}{r^2}\frac{\partial}{\partial r}\left(r^2 \rho_g D_{i,g}\frac{\partial Y_i}{\partial r}\right) + S_i \tag{7}$$

$$\rho_g c_{p,g}\frac{\partial T_g}{\partial t} + \rho_g u_r \frac{\partial h_g}{\partial r} = \frac{1}{r^2}\frac{\partial}{\partial r}\left(r^2 \lambda_g \frac{\partial T_g}{\partial r}\right) + S_h \tag{8}$$

Spherical symmetry gives the following boundary conditions at the center of the domain ($r = 0$):

$$u_r(0) = \frac{\partial T_g}{\partial r}(0) = \frac{\partial Y_i}{\partial r}(0) = 0 \tag{9}$$

Fourier-type boundary conditions are used at the external limit of the domain ($r = r_2$):

$$\frac{\partial T_g}{\partial r}(r_2) = h'_T\left(T_{g,\infty} - T_{g,2}\right) \tag{10}$$

$$\frac{\partial Y_i}{\partial r}(r_2) = h'_i\left(Y_{g,\infty} - Y_{g,2}\right) \tag{11}$$

$$h'_i = h'_T = \frac{r_2}{2t}\frac{\rho_g c_{p,g}}{\lambda_g} \tag{12}$$

Interaction with the dispersed phase is represented by the following source terms:

$$S_\rho = \dot{\rho}_{F,v} \tag{13}$$

$$S_i = \left(\delta_{i,F} - Y_i\right)\dot{\rho}_{F,v} + \dot{\rho}_{i,\chi} \tag{14}$$

$$S_h = \dot{H}_v - \dot{\rho}_{F,v}\cdot h_{F(g)} - \sum_{i\in\chi}\dot{\rho}_{i,\chi}h_i \tag{15}$$

The dilute spray is represented by a set of N_d classes, with each class having a droplet diameter d_k and a number density n_k. Evaporation source terms are deduced from the evaporation mass flow-rate $\dot{m}_k$ and heat flux $\dot{q}_k$, for each size class. Those exchange parameters are computed using the infinite conduction

model proposed by Sirignano [4]. In this first version of the model, droplets are fixed in space.

$$\dot{\rho}_{F,v} = \sum_{k=1}^{N_d} n_k \dot{m}_k \tag{16}$$

$$\dot{H}_v = \sum_{k=1}^{N_d} (n_k \dot{m}_k h_k - n_k \dot{q}_k) \tag{17}$$

Combustion is represented by the following one-step chemical reaction:

$$C_{10}H_{22} + \frac{31}{2} O_2 \xrightarrow{\dot{\omega}} 10CO_2 + 11H_2O, \tag{18}$$

and an Arrhenius-type reaction rate, with non-unity reaction orders relative to *n*-decane and oxygen, as proposed by Westbrook and Dryer [5]:

$$\dot{\omega} = B \cdot \exp\left[-\frac{T_a}{T_g}\right] \cdot \left[\frac{\rho_g Y_F}{M_F}\right]^{0,25} \cdot \left[\frac{\rho_g Y_{O_2}}{M_{O_2}}\right]^{1,5} \tag{19}$$

Finally,

$$\dot{\rho}_{i,\chi} = M_i \nu_i \dot{\omega}. \tag{20}$$

Further details can be found in García Rosa [3].

PARAMETRIC STUDY ON KERNEL GROWTH

An example of kernel growth is plotted on Figure 10. The initial conditions (t = 0) represent the spark plug used in the experimental study ($r_1 \approx 5.1$ mm, $T_1 = 3500$ K). The computational domain extends to $r_2 > 3r_1$, to reduce the influence of boundary conditions. Ambient and initial conditions are 300 K and 1.013 bar. In this example, the mixture is gaseous and the composition is defined by an equivalence ratio of 0.5. Flame speed is then estimated to be 36 cm/s.

This example shows what can be called a successful kernel formation. From here, we can define a criterion for successful kernel ignition and the ignition delay, as the time at which the flame front reaches a radius of 2 r_1.

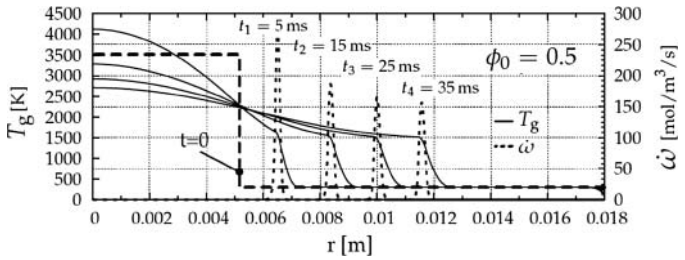

Figure 10 Example of kernel growth.

Gaseous and Monodisperse Mixtures

A parametric study has been conducted to compare the kernel ignition behavior between gaseous and monodisperse mixtures. In the case of two-phase mixtures, the initial gaseous mixture is only air, with the fuel being initially in the liquid phase only. Under these conditions, the liquid equivalence ratio can be defined as

$$\phi_{\ell,k} = \frac{n_k \rho_k \frac{\pi d_k^3}{6}}{\rho_{g,\infty} \cdot \alpha_s} \tag{21}$$

where α_s is the stoichiometric fuel-to-air mass ratio.

Figure 11 compares the ignition delay versus equivalence ratio curves for different monodisperse mixtures and the gaseous mixture. The results regarding the gaseous mixtures display the well-known nonmonotonic evolution, with a minimum ignition delay (corresponding to a maximum flame speed) for stoichiometric conditions. However, the rich extinction limit is very largely overestimated, due to the simplicity of the chemical kinetics scheme. The results for the different monodisperse mixtures show the same nonmonotonic behavior as demonstrated by Aggarwal [6] and Sirignano [4]. It can be observed that minimum ignition delay increases with droplet size. However, it is important to mention that as the droplet size decreases, the ignition behavior is totally different from that of the gaseous mixture. This is probably due to the definition of the liquid equivalence ratio. Indeed, ϕ_ℓ is defined, in Eq. (21), at temperature T_∞. With the evaporation process taking place at a higher temperature, the mass of air surrounding the droplets is lower than expected, and the resulting liquid equivalence ratio is higher.

These results show that, for the smallest droplets, at a moderate equivalence ratio ($\phi_\ell \approx 1.5$) the high evaporation rate induces a higher gaseous equivalence ratio and a rapid decrease in gas temperature, leading to an increasing ignition delay. On the other hand, for larger droplets ($d_k > 80$ μm) at a moderate and even higher equivalence ratio, the lower evaporation rate leads to a lower local gaseous equivalence ratio. The resulting gaseous mixture is therefore within the flammability limits and the ignition delay remains low.

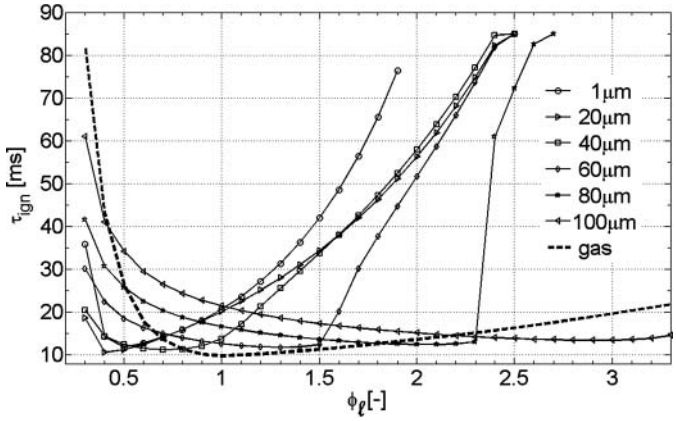

Figure 11 Influence of droplet size on ignition delay.

Table 1 Mass fraction distribution for polydisperse mixture of Figure 10

Size class (μm)	13	18	33	39
Mass fraction	**0.08**	**0.46**	**0.30**	**0.16**

Polydisperse Mixtures

Figure 12 presents an example result of the kernel formation in a polydisperse mixture, with four size classes. The two plots show the transit of the flame front at the ignition criterion $r = 2r_1$. The flame front can be identified on curves of gas temperature and reaction rate. As can be seen on the upper graph, the evaporation of the different droplets is staged. The smallest droplets are evaporated inside the preheat zone, whereas the largest are evaporated in the reactive zone of the flame front. In this case, the liquid equivalence ratio is equal to 1. The fuel mass distribution is nonuniform, as shown in Table 1.

A second parametric study was conducted to compare the ignition behavior of bidisperse and monodisperse mixtures. A bidisperse mixture, composed of 25- and 50-μm droplets in equal mass proportions, is compared to three monodisperse mixtures (Figure 13). The first has a droplet diameter equal to the arithmetic mean diameter ($d_{10} = 37.5$ μm); the second, equal to the surface mean diameter ($d_{20} = 39$ μm); and the third, equal to the Sauter mean diameter ($d_{32} = 45$ μm). This kind of comparison was first presented by Aggarwal and Sirignano [7]. Indeed, the authors have shown that the d_{20} mixture fitted the best the behavior of the bidisperse mixture, whereas the d_{32} overestimated ignition delay at low equivalence ratio. Although these results diverge from the observations by Aggarwal and Sirignano [7] at low equivalence ratio, the ignition delays of the different mixtures converge to the same value at high equivalence ratio, as observed by the authors.

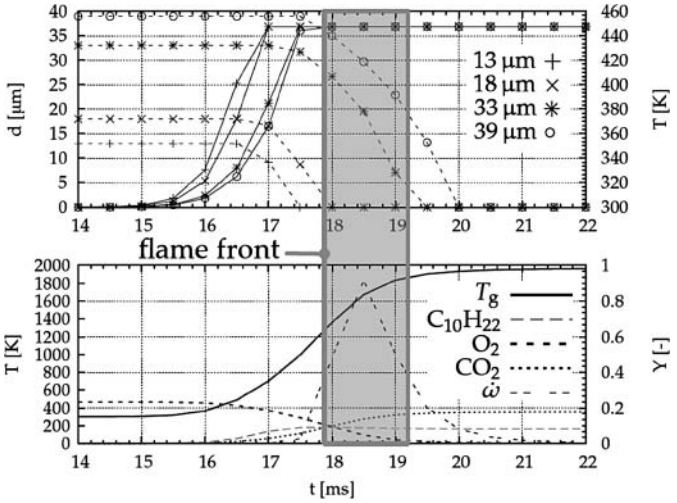

Figure 12 Temporal evolution of the gas and droplet parameters during the flame transit at the ignition criterion ($r = 2\ r_1$).

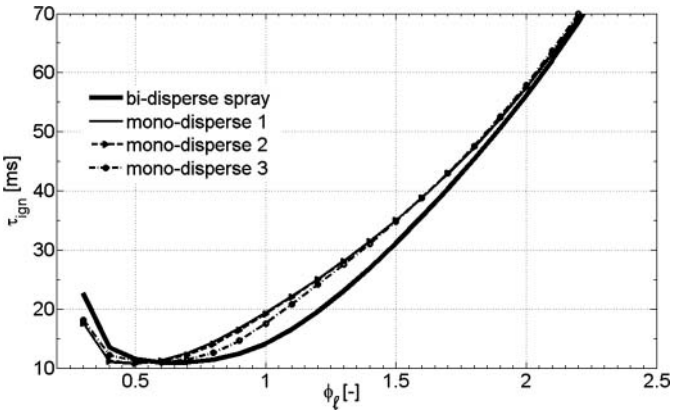

Figure 13 Ignition delay versus equivalence ratio for a bidisperse mixture compared to monodisperse.

KERNEL PROPAGATION IN A MODEL COMBUSTOR

Three-dimensional RANS Euler–Lagrange numerical simulations of the two-phase flow inside the model combustor were conducted, to analyze kernel transport, after a successful formation. The nonreactive spray structure was first validated against LDA, PDA, and PIV measurements. Then reactive flow simulations were compared to the experimental ignition tests. The computational mesh features all the details of the injector air plenum and swirler, to simplify boundary conditions, and initial conditions for the disperse phase are given by PDA measurements. Operating conditions are ambient pressure, 463 K air temperature (hotter than ambient, for the sake of optical access), 15 g/s air mass flow rate, and 1 g/s kerosene mass flow rate.

Structure of the Spray Before and After Ignition

Figure 14 shows a qualitative comparison between the computed and observed spray structure. The simulation results show the kerosene evaporated mass fraction field, as well as the droplet size. Although RANS simulations fail to reproduce the

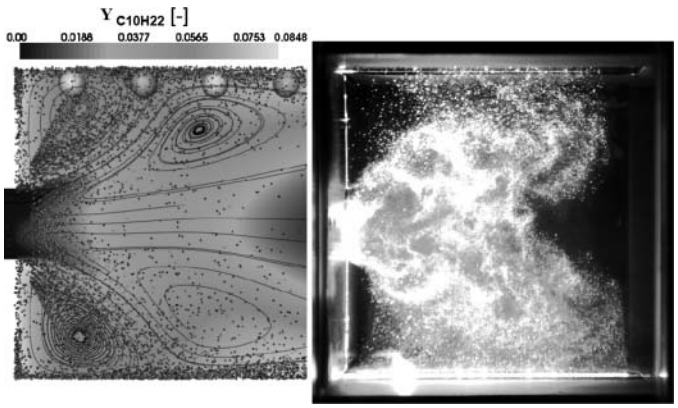

Figure 14 Laser sheet visualization (right) and 3D RANS simulation (left; see text for details) of the spray before ignition.

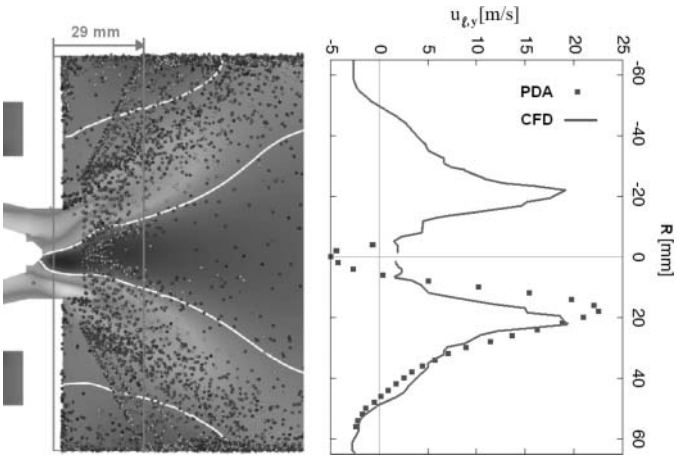

Figure 15 Simulated droplet axial velocity profile vs. experimental (PDA) measurements.

complex structures observed in the instantaneous visualization, both approaches show the same mean characteristics: center and corner recirculation zones, hollow-cone shaped spray, spray expansion, impingement position on windows, and mean droplet velocity near the injector (Figure 15).

Kernel Propagation

Figure 16 recalls the preliminary results obtained by Ouarti [8] in a two-dimensional (2D) axisymetric mesh of the same model combustor geometry. The results of Ouarti are particularly interesting because successful and failed ignition cases coincide with the experiments.

This case shows the diffusion and transport of the kernel toward the corner recirculation zone, where it stabilizes. The relatively slow propagation is representative of a transitional case. Indeed, a lower equivalence ratio leads to flame blow-out, as observed in both experimental (Figure 7) and numerical results [8]. Although the preliminary results display a good agreement with experiments, it is important to note that a spherical kernel

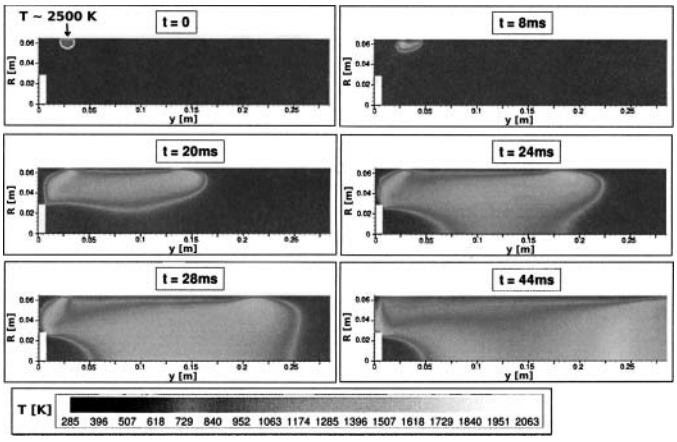

Figure 16 Temporal evolution of temperature field during kernel transport and subsequent combustor ignition (injected equivalence ratio 1.75 [8]).

deposition cannot be represented in an axisymmetric geometry. Three-dimensional reactive-flow simulations are currently under development and results will be presented in a future paper.

CONCLUSIONS AND PERSPECTIVES

A new in-depth experimental database was obtained on the MERCATO test bench, through the use of optical diagnosis. This data were used to build a 1D ignition kernel model, with several improvements with respect to previous work [8]: namely, a parametric study comparing gaseous, monodisperse, and polydisperse mixtures was conducted to better understand flame propagation mechanisms in two-phase flows. Encouraged by the first results on a 2D axisymmetric configuration, this work developed a detailed comparison between experiments and 3D simulations. Moreover, the presented model is being put into practice by TURBOMECA on real combustors. Results show that this can be used to optimize the igniter position and encourage future work on the experimental validation and further investigation of the kernel propagation process.

NOMENCLATURE

c_p	constant-pressure heat capacity, J/K/kg
D	molecular diffusion coefficient, m^2/s
d	droplet diameter, m
d_{10}	arithmetic mean diameter, m
d_{20}	diameter of average surface, m
d_{32}	Sauter mean diameter, m
E	energy, J
h	mass enthalpy, J/kg
h'	global exchange coefficient, 1/m
$\dot{H}$	enthalpy source term, J/kg/s
M	molar weight, kg/mol
m	mass, kg
n	number density, $1/m^3$
N_d	number of droplet classes, dimensionless
p	pressure, Pa
$\dot{q}$	heat power, W
r^0	ideal gas constant for air, $r^0 = 287.14$ J/kg/K
r	ignition kernel radius, m
R	radial coordinate, m
y	axial coordinate, m
S_i	mass fraction source term, $kg/m^3/s$
S_h	enthalpy source term, J/kg/s
S_ρ	mass source term, $kg/m^3/s$
T	temperature, K
T_a	activation temperature, K
t	time, s
u_r	radial component of gas velocity, m/s
u_y	axial component of velocity, m/s

Y mass fraction, dimensionless
Z compressibility factor, dimensionless

Greek Symbols

α fuel-to-air mass ratio, dimensionless
χ species list $\chi = \{C_{10}H_{22}, O_2, CO_2, H_2O, N_2\}$
λ thermal conductivity, W/m/K
ν stoichiometric coefficient, dimensionless
$\dot{\omega}$ molar reaction rate, mol/m^3/s
φ equivalence ratio, dimensionless
ρ density, kg/m^3
$\dot{\rho}$ mass source term, kg/m^3/s
τ_{ign} ignition delay, s

Subscripts

χ relative to chemical reactions
F relative to fuel ($F = C_{10}H_{22}$)
g relative to the gas phase
(g) relative to the gaseous state
i relative to species i of list χ
∞ conditions far from the control volume
k relative to class of size d_k
ℓ liquid
s relative to stoichiometric conditions
spk relative to the spark
v relative to evaporation phenomena
0 before spark discharge
1 after spark discharge
2 at boundary of the computational domain

REFERENCES

Lefebvre, A. W., *Gas Turbine Combustion*, Hemisphere, New York, 1983.

Thiele, M., Selle, S., Riedel, U. Warnatz, J., and Maas, U., Numerical Simulation of Spark Ignition Including Ionization, *Proceedings of the Combustion Institute*, vol. 28, pp. 1177–1185, 2000.

García Rosa, N., *Phénomènes d'allumage d'un foyer de turbomachine en conditions de haute altitude, Ph.D. thesis*, Université de Toulouse, 2008.

Sirignano, W. A., *Fluid Dynamics and Transport of Droplets and Sprays*, Cambridge University Press, Cambridge, UK, 1999.

Westbrook, C. K., and Dryer, F. L., Simplified Reaction Mechanisms for the Oxidation of Hydrocarbon Fuels in Flames, *Combustion Science and Technology*, vol. 27, pp. 31–43, 1981.

Aggarwal, S. K., A Review of Spray Ignition Phenomena: Present Status and Future Research, *Progress in Energy and Combustion Science*, vol. 24, pp. 565–600, 1998.

Sirignano, W. A., and Aggarwal, S. K., Ignition of Polydisperse Sprays: Importance of d20, *Combustion Science and Technology*, vol. 46, pp. 289–300, 1986.

Ouarti, N., Lavergne, G., and Lecourt, R., Modeling of the Ignition Inside a Turbojet Combustor. Application to In-Flight Relight, ILASS 2004, Nottingham (Grande Bretagne), 6–8 September, 2004.

Guillaume Linassier is a Ph.D. student at ONERA/DMAE (Research Group on Multiphase Flows), Toulouse, France, under the supervision of Prof. He obtained his M.Sc. degree in 2008 at Ecole Centrale de Lyon, France. He is currently working on two-phase combustion and ignition in a turbojet combustor.

Nicolás García Rosa is a researcher at ISAE (Aerodynamics, Energetics and Propulsion department). He received his Ph.D. in fluid mechanics in 2008 from Université de Toulouse, France. He previously worked on two-phase ignition and is currently in charge of experimental platforms and projects on turbo machine aerothermodynamics.

Renaud Lecourt is a researcher at ONERA/DMAE (Research Group on Multiphase Flows). He is currently in charge of experimental facilities and projects on two-phase combustion in air breathing engine combustors, and more specifically on spray ignition in critical conditions. He previously worked on injection systems for liquid-propellant rocket engines.

Philippe Villedieu is a senior researcher at ONERA/DMAE (Research Group on Multiphase Flows) and a professor of applied mathematics at INSA, Toulouse, France. He works on the numerical modeling of two-phase flows and is currently in charge of the development of the dispersed-phase Lagrangian solver in the multiphysics code, CEDRE, developed by ONERA.

Gerard Lavergne received his Ph.D. in fluid mechanics in 1978, from University of Toulouse, France. He is a professor at ISAE/SUPAERO formation in the DAEP department, and is an HDR (habilité à diriger les recherches), and director of research at ONERA. He has been involved in two-phase flow research for the past 30 years. He established the Heterogeneous Multiphase Flow Research Unit in 1997. His research is oriented toward the modeling of the physical processes occurring in dilute and dense two-phase flows. The main application of this work is fuel injection in combustion chambers.